



**HAL**  
open science

## 5000 yr of paleoseismicity along the southern Dead Sea fault

Y Klinger, M Le Béon, M Al-Qaryouti

► **To cite this version:**

Y Klinger, M Le Béon, M Al-Qaryouti. 5000 yr of paleoseismicity along the southern Dead Sea fault. Geophysical Journal International, 2015, 10.1093/gji/ggv134 . insu-01301716

**HAL Id: insu-01301716**

**<https://insu.hal.science/insu-01301716>**

Submitted on 12 Apr 2016

**HAL** is a multi-disciplinary open access archive for the deposit and dissemination of scientific research documents, whether they are published or not. The documents may come from teaching and research institutions in France or abroad, or from public or private research centers.

L'archive ouverte pluridisciplinaire **HAL**, est destinée au dépôt et à la diffusion de documents scientifiques de niveau recherche, publiés ou non, émanant des établissements d'enseignement et de recherche français ou étrangers, des laboratoires publics ou privés.

## 5000 yr of paleoseismicity along the southern Dead Sea fault

Y. Klinger,<sup>1</sup> M. Le Béon<sup>2</sup> and M. Al-Qaryouti<sup>3</sup>

<sup>1</sup>*Institut de Physique du Globe de Paris, Sorbone Paris Cité, Université Paris Diderot, UMR F-7154 CNRS, Paris, France. E-mail: [klinger@ipgp.fr](mailto:klinger@ipgp.fr)*

<sup>2</sup>*Department of Geosciences, National Taiwan University, Taipei, Taiwan*

<sup>3</sup>*Jordan Seismological Observatory, Ministry of Energy and Mineral Resources, Amman, Jordan*

Accepted 2015 March 18. Received 2015 March 16; in original form 2014 October 8

### SUMMARY

The 1000-km-long left-lateral Dead Sea fault is a major tectonic structure of the oriental Mediterranean basin, bounding the Arabian Plate to the west. The fault is located in a region with an exceptionally long and rich historical record, allowing to document historical seismicity catalogues with unprecedented level of details. However, if the earthquake time series is well documented, location and lateral extent of past earthquakes remain often difficult to establish, if only based on historical testimonies. We excavated a palaeoseismic trench in a site located in a kilometre-size extensional jog, south of the Dead Sea, in the Wadi Araba. Based on the stratigraphy exposed in the trench, we present evidence for nine earthquakes that produced surface ruptures during a time period spanning 5000 yr. Abundance of datable material allows us to tie the five most recent events to historical earthquakes with little ambiguities, and to constrain the possible location of these historical earthquakes. The events identified at our site are the 1458 C.E., 1212 C.E., 1068 C.E., one event during the 8th century crisis, and the 363 C.E. earthquake. Four other events are also identified, which correlation with historical events remains more speculative. The magnitude of earthquakes is difficult to assess based on evidence at one site only. The deformation observed in the excavation, however, allows discriminating between two classes of events that produced vertical deformation with one order of amplitude difference, suggesting that we could distinguish earthquakes that started/stopped at our site from earthquakes that potentially ruptured most of the Wadi Araba fault. The time distribution of earthquakes during the past 5000 yr is uneven. The early period shows little activity with return interval of  $\sim 500$  yr or longer. It is followed by a  $\sim 1500$ -yr-long period with more frequent events, about every 200 yr. Then, for the past  $\sim 550$  yr, the fault has switched back to a quieter mode with no significant earthquake along the entire southern part of the Dead Sea fault, between the Dead Sea and the Gulf of Aqaba. We computed the Coefficient of Variation for our site and three other sites along the Dead Sea fault, south of Lebanon, to compare time distribution of earthquakes at different locations along the fault. With one exception at a site located next to Lake Tiberias, the three other sites are consistent to show some temporal clustering at the scale of few thousands years.

**Key words:** Palaeoseismology; Continental tectonics: strike-slip and transform; Dynamics and mechanics of faulting; Dynamics: seismotectonics.

### INTRODUCTION

The 1000-km-long left-lateral Dead Sea fault (Fig. 1) marks the boundary between the Arabian Plate and the Sinai block (Quennell 1959; Freund *et al.* 1968; Garfunkel *et al.* 1981; Klinger *et al.* 2000a). The fault is mostly linear, trending N5°E–N10°E, with only a few noticeable extensional steps such as the Hula basin (Heimann & Ron 1993) and the Dead Sea basin (Garfunkel 1981; Ben Avraham 1992), and one major bend in its central section, in Lebanon. There, the Dead Sea fault bends eastward about 20°, to form a major transpressional step with

the motion partitioned between the on-shore Yammounch strike-slip fault and the off-shore thrust faults (Daëron *et al.* 2005; Daëron *et al.* 2007; Elias *et al.* 2007). Mount Lebanon, resulting from this bend, tops at 3090 m. Along the central and southern sections, the slip rate has been estimated at several places, and over various timescales, from few years to several hundred thousands of years. Results converge around an average value of  $5 \pm 2$  mm yr<sup>-1</sup> (Klinger *et al.* 2000a; Niemi *et al.* 2001; Daëron *et al.* 2004; Marco *et al.* 2005; Gomez *et al.* 2007; Le Béon *et al.* 2008, 2010, 2012; Makovsky *et al.* 2008; Ferry *et al.* 2011). North of Lebanon, however, slip rates estimated over different

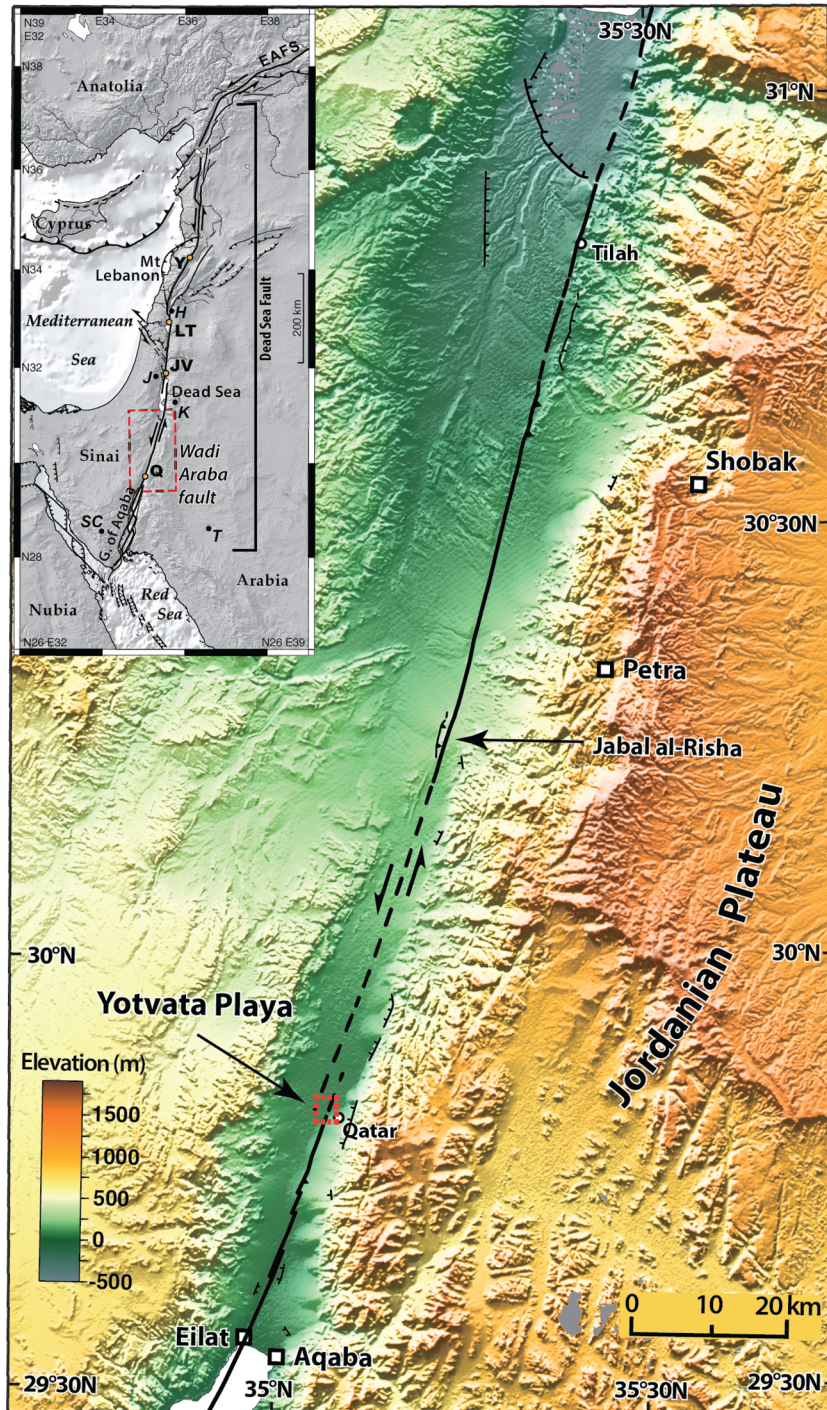


**Figure 1.** Inset map shows the entire Dead Sea fault, including major relay zones of the Dead Sea basin and the Lebanese bend. Y, LT, JV and Q indicate paleoseismological sites of Yammouneh, Lake Tiberias, Jordan Valley and Qatar, respectively. T, K, J, H and SC indicate cities of Tabuk, Al-Karak, Jerusalem, Hula basin and St Catherine monastery, respectively. EAFS stands for East Anatolia Fault System. The main figure shows the Wadi Araba fault segments after (Le Béon *et al.* 2012), with location of the trench site in Yotvata Playa. The site of Tilah is also indicated. Dashed red box indicates Fig. 2. Topography from SRTM3 (pixel size,  $\sim 90$  m).

timescales, from present-day using GPS to historical times, diverge significantly, with values ranging from 2 to 6 mm yr<sup>-1</sup> (Meghraoui *et al.* 2003; Alchalbi *et al.* 2010).

Large earthquakes ( $M > 7$ ) have ruptured different sections of the fault (Abou Karaki 1987; Ambraseys *et al.* 1994; Guidoboni *et al.* 1994; Guidoboni & Comastri 2005; Ambraseys 2009; Agnon 2014; Marco & Klinger 2014). Since the Antiquities, many of these

earthquakes have been recorded in the historical accounts, based on damages and fatalities reported to the local authorities. Although such historical basis is useful to get an insight into the fault behaviour, it puts the preeminence on populated areas and it could eventually lead to the mislocation of historical earthquakes. This issue is particularly sensitive for the Wadi Araba fault segment of the Dead Sea fault, which is located between the Dead Sea basin





**Figure 3.** Field view of the pressure ridge, about 50 cm high, popping up in the lake sediments of the Yotvata playa.

Note that E and H correspond to packages of several related units rather than to a single unit. These units are used as reference to discuss event horizons in the following sections.

Based on units bends and offsets and fault cracks, two zones of active deformation can be identified in the trench, about 9 m apart. The main fault zone (Fig. 5) is 8 m wide and is located in the western part of the trench, between the Meter Mark (MM) 1 and MM9. Although the trench extends several more metres westward, no additional deformation could be observed west of MM1. The main deformation zone is located around MM6 where most of the sedimentary units drop down to the east. A minimal vertical motion of about 65 cm could be estimated, based on units that can be traced across the fault zone. The deformation is accommodated by numerous faults vertically offsetting the units, in addition to significant warping of the entire sedimentary pile up to unit D. The accommodation space created east of the main fault zone is filled by a sedimentary sequence, beneath unit C, about 1 m thick that is only present in a very condensed way in the western part of the trench. This additional sedimentary body is characterized by abundant evidence for channels flowing perpendicular to the trench. Scour marks, erosional contacts, coarser sand channels and silt lenses can be observed that testify that the water running down from the alluvial fans was forced to flow northward, limited to the west by a tectonic scarp. A series of nested channels is actually visible just east of the main fault zone, between MM6 and MM9. Such discontinuous stratigraphy and the presence of several channels make the recognition of tectonic cracks more difficult in this section.

The secondary zone of faulting is located about 9 m east from the main fault zone, between MM16 and MM25, and is mostly characterized by vertical cracks with only limited evidence of vertical offset (Fig. 5).

### Description of earthquake ruptures

The identification of earthquake ruptures is mostly based on consistent upward terminations of sets of cracks that vertically offset

sedimentary units (McCalpin 1996). Horizontal motion is more difficult to recognize when sedimentary unit thickness is similar over a large area, as expected in playa deposits. In addition, in our trench the medium to coarse grain size of many sandy units makes it more difficult to definitely identify the exact location of some of the cracks termination (Fig. S1). Hence, our analysis focuses only on the large events that have extensively ruptured the ground surface at the trench site, and are responsible for primary deformation and/or cracking. Significant ground ruptures involve that the magnitude associated to these events is most probably  $M_w \sim 6.5$  or above (McCalpin 1996), when the entire thickness of the brittle crust would rupture. In this respect, as we benefitted from rich stratigraphy and do not have massive homogeneous layer in excess of 10–15 cm thickness, at least in the main fault zone, it is very unlikely that we could miss any major event. Smaller magnitude earthquakes responsible for limited surface ruptures, or secondary faulting related to distant earthquakes, might also be visible in the trench. At this stage, however, the lack of congruent observations in the trench prevents us from discussing them further in details.

Nine earthquakes have been identified unambiguously in our trench, which are named E1–E9, with E9 being the oldest (Fig. 5). All of them involve deformation and cracks in the main fault zone. Events E5, E7, E8 and E9 are not visible in the eastern fault zone, either because they did not actually produce any rupture in this area or because the broken layers are too deep to be exposed. Two additional events are loosely constrained, including one earthquake visible in the eastern fault zone only (labelled *Esupp1* in Fig. 5). Here, we summarize the information regarding the identification of the 9 main events and we discuss the evidence that could potentially relate to the two additional earthquakes.

From the bottom of the trench a set of two faults are identified that offset the lower part of unit H at MM5. The upper end of these two cracks is not well defined, but the sandier units above them, which alternate with finer material to form unit H, are not offset, forcing the event horizon E9 to be below the sand.

The event E8 is characterized by the tilting of layers of unit H along a set of distinctive faults, most of them dipping westward,

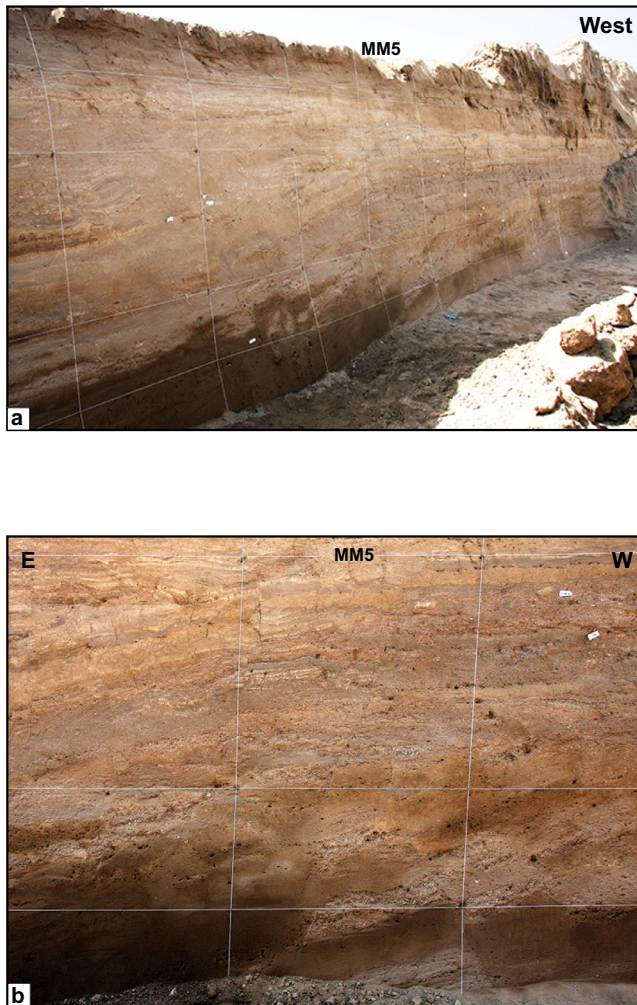


**Figure 4.** (a) Overview of the south wall of the trench. Numerous distinct layers of sand and silt are visible. The thinning of the whitish silt westwards corresponds to the main deformation zone with significant downdrop of the east compartment. White squares are 1 m aside for scale. (b) Zoom on the stratigraphy at meter mark MM5 (Fig. 5). Faults are visible that offset the yellowish silt and grey sand layers in the upper part of the photograph. Rotated blocks are also visible in the lower part.

between MM1 and MM5. Such tilt was probably also accompanied by a significant down-drop of the eastern compartment that created some accommodation space later filled by the horizontal units visible at the bottom of the trench east of MM8, below unit G. Upward terminations of faults associated to event E8 are located at the contact between H and G. However, the contact between H and G is not offset by these faults, unlike the lower layers, suggesting that the contact between H and G corresponds to an erosional contact postdating event E8, and is not the actual event horizon associated with the event E8 (E8 is indicated in Fig. 5 only for reference, at the same level as E7; see below). Some of the cracks associated to the event E8 can be continued through the upper layers as later events triggered slip on these cracks and made them propagate upward. The geometry of the upper part of these cracks, however, is totally different as they dip eastward, in agreement with the geometry of the faults associated to more recent earthquakes.

A liquefaction conduit is visible between MM5 and MM6. It is tilted, similarly to all the layers of unit H, implying that it predates E8, but it goes much higher than the two cracks identified at MM5

and associated to E9, indicating that it has to postdate E9. Hence, this conduit and the faint cracks that affect the same level, visible at MM3 and between MM5 and MM6, might be the evidence for an additional rupturing event, named *E<sub>supp2</sub>*, sometime between E8 and E9, that remains difficult to document further at that stage.

The next event, E7, is defined by the set of faults below MM5, that dip eastward or westward and offset the top of unit H, although most of them do not propagate into G. These faults also offset the liquefaction conduit close to its base. Most of the faults related to E7 are sealed by G. Hence, the E7 event horizon has to be at the boundary between H and G. This makes it difficult to clearly distinguish event horizons associated, respectively, to E8 and E7. Some other faults, also activated during E7, were reused by later ruptures that lead to larger cumulative vertical offset in the lower part of the trench compared to the upper part.

The event E6 corresponds to a group of faults that ends in unit G. These faults are well visible at MM1, MM6–MM7 and at MM17. The fact that the upward termination of these faults is not always at the same level is probably due to the lateral change in thickness of G, mostly notable at MM7 in the main fault zone. Such change in thickness is interpreted as a combination of deposition-thickness change, due in part to down-drop of the eastern compartment during the previous event E7, and to the effect of horizontal offset during E6. The event horizon for E6 is conservatively located at the contact between G and F, although it might be lower in the section, if one considers that the one crack at MM7 that ends at the F–G contact might not be part of E6, but would be related to a latter crack that propagated higher and was then truncated by subsequent erosion/deposition.

Event E5 is characterized by limited deformation, well identified at MM3 based on faults that end at the top of unit E and are sealed by unit D. Unit D is a yellowish compact fine sand layer with sharp limits that allow for unambiguous identification of any rupture that would offset this unit. Hence, at MM5 the faults that rupture unit D and stop just above D cannot be E5 and are related to the next event E4. The unit E can be traced across the entire trench and no cracks related to E5 are visible east of MM8.

Event E4 likely was a major event that caused a significant down-drop of the eastern compartment relative to the western part. When adding vertical offsets for all cracks that affect unit D between MM5 and MM8 and off-fault warping, the actual vertical motion reaches 65 cm. In the main fault zone, at MM7, deformation of the layers suggests local compression in addition to the main strike-slip motion, resulting in a metre-size pressure ridge. This feature was later eroded and only partial evidence can now be recognized.

The accommodation space created on the eastern side of the trench during the event E4 was filled by sediments. Unlike previous units, most of this sediment package is formed by numerous thin cross-bedded layers and channels, formed by silt to sand, with only little lateral continuity. This package, up to unit C, is onlapping the palaeo-fault scarp formed during E4, making recognition of specific layers across the main fault zone difficult. Only three layers in the upper part of the onlap strata and above it, units A, B and C, can be traced across the entire trench with confidence.

Within this sedimentary fill, some of the cross-bedded layers onlapping unit D at MM6 and MM7 are affected by two cracks that distinctly stop just below the major channel visible between MM7 and MM9. Some cracks at MM5 also offset D. They can be traced a few centimetres higher to end at a level consistent with the end of the cracks located between MM7 and MM9. All these cracks define the event E3.

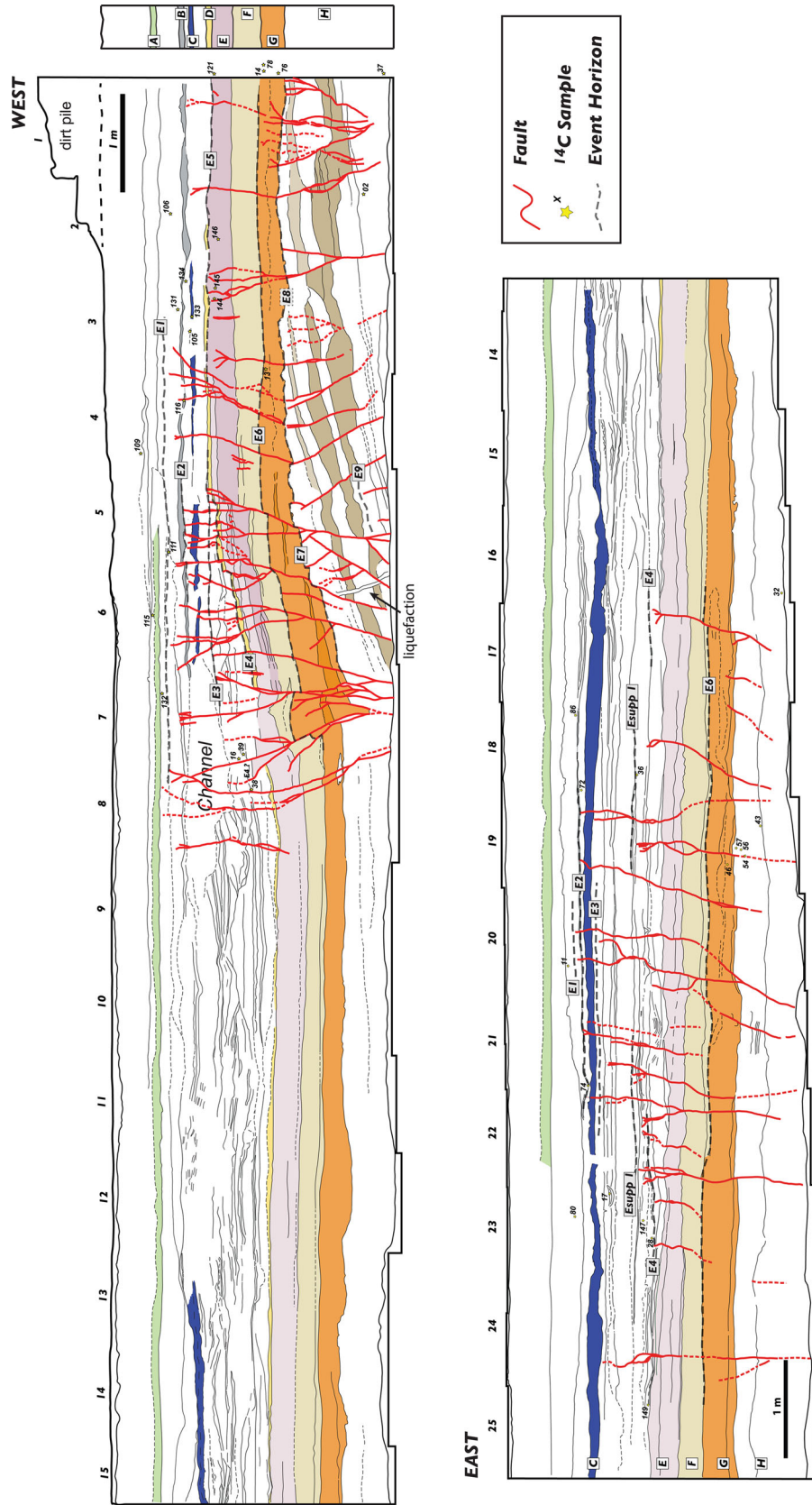


**Figure 5.** Trench log of the southern wall. The full resolution photomosaic of the wall is available in Fig. S1. The different stratigraphic units are indicated by letters A to H located in the synthetic stratigraphic section. Conservative position of event horizons are indicated with a dashed line, including for event *Esupp 1* unambiguously visible in the eastern fault zone only. E8 is indicated for reference, although the dashed line corresponds to E7 event horizon (see discussion in text). *Esupp 2*, between E8 and E9 is not indicated. Meter Marks (MM) are indicated above the trench. Dated <sup>14</sup>C samples are indicated by star. To the west, a few samples have been collected up to 2 m outside the gridded wall, where the layers could be traced horizontally. Samples are indicated at the corresponding depth and stratigraphic position.

**Table 1.** Mass Spectroscopy measurements were made at the Keck carbon cycle mass spectroscopy facility at University of California, Irvine. Ages were calibrated using OxCal 4.2 (Bronk-Ramsey 2009) and calibration curve INTCAL13 (Reimer *et al.* 2013). Calibrated ages are indicated in Common Era (CE) or Before Common Era (BCE).

Sample name	Reporting number	Fraction modern	±	$\delta^{14}\text{C}$ (‰)	±	$^{14}\text{C}$ age (BP)	±	Modelled calibrated age ( $\pm 2\sigma$ )
QT09-02	UCIAMS 119520	0.5951	0.0012	-404.9	1.2	4170	20	2816 BCE–2633 BCE
QT09-11	UCIAMS 88945	0.9470	0.0016	-53.0	1.6	440	15	1438 CE–1462 CE
QT09-13	UCIAMS 73378	0.7656	0.0020	-234.4	2.0	2145	25	231 BCE–61 BCE
QT09-14	UCIAMS 73379	0.7609	0.0018	-239.1	1.8	2195	20	314 BCE–178 BCE
QT09-16	UCIAMS 119521	0.8718	0.0014	-128.2	1.4	1100	15	895 CE–988 CE
QT09-32.040 mgC	UCIAMS 88946	0.6771	0.0097	-322.9	9.7	3130	120	1613 BCE–1171 BCE
QT09-37.083 mgC	UCIAMS 73380	0.6067	0.0028	-393.3	2.8	4015	40	2861 BCE–2644 BCE
QT09-38.069 mgC	UCIAMS 119522	0.7926	0.0026	-207.4	2.6	1870	30	73 CE–227 CE <sup>a</sup>
QT09-39	UCIAMS 119523	0.8708	0.0016	-129.2	1.6	1110	15	893 CE–981 CE
QT09-43	UCIAMS 119524	0.6908	0.0011	-309.2	1.1	2970	15	1255 BCE–1124 BCE
QT09-46.063 mgC	UCIAMS 88947	0.7578	0.0045	-242.2	4.5	2230	50	316 BCE–116 BCE
QT09-54	UCIAMS 88948	0.7568	0.0014	-243.2	1.4	2240	15	385 BCE–236 BCE
QT09-56	UCIAMS 88949	0.7377	0.0013	-262.3	1.3	2445	15	389 BCE–248 BCE
QT09-72	UCIAMS 88950	0.8967	0.0015	-103.3	1.5	875	15	1055 CE–1215 CE
QT09-76	UCIAMS 73381	0.7324	0.0017	-267.6	1.7	2500	20	772 BCE–540 BCE <sup>a</sup>
QT09-78	UCIAMS 73382	0.7802	0.0019	-219.8	1.9	1995	20	45 BCE–53 CE
QT09-80	UCIAMS 88951	0.9480	0.0016	-52.0	1.6	430	15	1441 CE–1474 CE
QT09-105	UCIAMS 73383	0.8689	0.0021	-131.1	2.1	1130	20	880 CE–981 CE <sup>a</sup>
QT09-106	UCIAMS 73384	0.9560	0.0022	-44.0	2.2	360	20	1476 CE–1624 CE
QT09-109	UCIAMS 73385	0.9868	0.0023	-13.2	2.3	105	20	1679 CE–1858 CE
QT09-111	UCIAMS 73386	0.9581	0.0021	-41.9	2.1	345	20	1458 CE–1601 CE
QT09-115	UCIAMS 73387	0.9731	0.0023	-26.9	2.3	220	20	1645 CE–1795 CE
QT09-116	UCIAMS 73388	0.9219	0.0022	-78.1	2.2	655	20	1281 CE–1385 CE
QT09-121	UCIAMS 73389	0.8246	0.0020	-175.4	2.0	1550	20	428 CE–560 CE
QT09-131	UCIAMS 73390	0.9504	0.0023	-49.6	2.3	410	20	1429 CE–1455 CE
QT09-132	UCIAMS 73391	0.9563	0.0026	-43.7	2.6	360	25	1501 CE–1641 CE
QT09-133	UCIAMS 73392	0.8704	0.0021	-129.6	2.1	1115	20	890 CE–982 CE <sup>a</sup>
QT09-134	UCIAMS 73393	0.8868	0.0021	-113.2	2.1	965	20	1027 CE–1155 CE
QT09-144	UCIAMS 73394	0.8469	0.0020	-153.1	2.0	1335	20	650 CE–691 CE
QT09-146	UCIAMS 73395	0.8292	0.0020	-170.8	2.0	1505	20	473 CE–614 CE
QT09-147	UCIAMS 88952	0.8561	0.0016	-143.9	1.6	1250	15	727 CE–873 CE
QT09-149	UCIAMS 88953	0.8511	0.0017	-148.9	1.7	1295	20	679 CE–770 CE

Notes: Radiocarbon concentrations are given as fractions of the Modern standard, D14C, and conventional radiocarbon age, following the conventions of (Stuiver & Polach 1977).

Sample preparation backgrounds have been subtracted, based on measurements of  $^{14}\text{C}$ -free wood.

All results have been corrected for isotopic fractionation according to the conventions of (Stuiver & Polach 1977), with  $\delta^{13}\text{C}$  values measured on prepared graphite using the AMS spectrometer. These can differ from  $\delta^{13}\text{C}$  of the original material, if fractionation occurred during sample graphitization or the AMS measurement, and are not shown.

<sup>a</sup>Samples that are out of stratigraphic order, most probably reworked. They are not included in the age model.

**Table 2.** Mass Spectroscopy measurements were made at the Scottish Universities Environmental Research Centre AMS Facility, Glasgow. Ages were calibrated using OxCal 4.2 (Bronk-Ramsey 2009) and calibration curve INTCAL13 (Reimer *et al.* 2013). Calibrated ages are indicated in Common Era (CE) and Before Common Era (BCE).

Sampling ID	Reporting number	$\delta^{13}\text{C}$ 0/00	$^{14}\text{C}$ age (BP)	$\pm 1\sigma$	Modelled calibrated age ( $\pm 2\sigma$ )
QT09-17	SUERC-27574	-25.1	995	35	975 CE–1115 CE
QT09-28	SUERC-27575	-27.1	1155	35	720 CE–860 CE
QT09-36	SUERC-27576	-22.3	1300	35	741 CE–887 CE
QT09-57	SUERC-27577	-27.0	2115	35	357 BCE–290 BCE
QT09-74	SUERC-27578	-23.3	795	35	1208 CE–1280 CE
QT09-86	SUERC-27579	-26.8	630	35	1296 CE–1405 CE
QT09-145	SUERC-27580	-25 (assumed)	1285	35	655 CE–730 CE

Despite the fact that we cannot definitively rule out the possibility that the numerous cracks ending at the same level on the eastern part of the trench wall, between MM18 and MM23, relate to E3, another event (labelled E<sub>supp1</sub> in Fig. 5) might tentatively be defined between E4 and E3. Although correlation remains difficult, it is likely that some of the faint cracks observed at MM6 and MM8 could relate to this event as well. Several of these cracks are not rooted and almost none of them display any significant offset, suggesting

that they may be only triggered cracks due to a distant earthquake or that they correspond to a local smaller magnitude earthquake (Liu-Zeng *et al.* 2013).

One of the few upper units that can be correlated across the entire trench is unit C. This unit is composed of medium sand with a characteristic pinkish colour. In many places secondary interfingering can be seen inside the unit and, in several locations, subsequent channels have eroded the top part of this unit. Just few centimetres

above unit C, one can also recognize unit B. Although more discontinuous, unit B is characterized by whitish silt to sand, varying in thickness from 1 to 10 cm. The thicker part of B is limited only to the western part of the trench. Because unit B is composed of fine laminated sediments, any crack breaking across it is easily recognizable. A distinct group composed of numerous cracks is mapped in the two fault zones that go through unit C, but are capped by unit B. This group of cracks defines the event E2 with the seismic horizon at the base of unit B. The cracks often branch out from previously formed fractures related to older events, at least in the western part of the trench. No significant vertical offset can be associated to any of them.

The event E1 is characterized by the group of fissures that break unit B. These fissures are quite numerous in the main fault zone, on the western side of the trench, but a few are also visible in the secondary fault zone. In the main fault zone, small vertical offset is associated to these cracks in several places. Defining the exact level of the event horizon associated with event E1 remains difficult as the upper part of the sedimentary section is characterized by channelling and flood deposits with limited lateral continuity. All the fissures, however, seem to end at approximately the same depth with reference to the current ground surface, allowing to define a pseudo-event-horizon for E1.

#### Age constraints and methods to determine the timing of events

Time constraints were derived from accelerator mass spectrometry (AMS) radiocarbon dating of detrital charcoals. The trench exposure proved to be unexpectedly rich in datable material and a total of 39 samples were dated (Tables 1 and 2). Only four samples had to be discarded, as they likely correspond to reworked samples yielding ages significantly older than other ages, relative to their stratigraphic position. The regular distribution of ages down to unit G (Fig. 6) confirms, in support to the logged section, that no major hiatus affects the stratigraphy and that the sedimentological record seems complete, especially for the last 2000 yr. For the earlier time period, because the contact between units H and G is erosional, up to 700 yr may be missing in the stratigraphy, making the earthquake record likely incomplete. The layers at the base of the trench date back to nearly 5 kyr BP.

Based on lateral continuity of several characteristic units across the trench, probability distribution of calendar ages for samples and event horizons have been determined following a Bayesian scheme (Bronk-Ramsey 2009), which accounts for relative stratigraphic positions of items (Fig. 6). However, because some vertical motion is involved that offset the eastern part of the section relative to the western part, in addition to dominant strike-slip motion, actual depth of each sample was not used to model ages. In several cases, phases have been defined to group samples that belong to the same unit and could not be clearly ordered based on vertical separation (Lienkaemper and Bronk-Ramsey 2009).

#### Identification of historical earthquakes and time window for earlier events

Overall, the Qatar record displays evidence for nine unambiguous paleoearthquakes and two additional events, more uncertain, over a period extending back to about 5 kyr BP. Within this time span, we have reasonable time constraints on an 'historical' sequence for the last 1700 yr, and fewer indications about the earthquake

activity during the earlier 'prehistoric' sequence. Hence, dates for individual events E1–E3, E6 and E7, are well constrained with several radiocarbon samples ( $^{14}\text{C}$ ) between each individual event horizon. The other identified events (E4 and E5) and (E8 and E9) interestingly appear to occur somehow by pair. The age of each pair is well constrained by several samples. If such pairing is a bias due to fewer samples in the lower section, or is real remains unclear. The latter possibility is explored in the discussion section.

The occurrence of the most recent event recorded at this site, E1, is tightly constrained from  $^{14}\text{C}$  dates to be between 1434 C.E. and 1459 C.E. During that interval, the only significant event reported in the area is a magnitude  $M6$  to  $M7$  event on 1458 November 16 (Abou Karaki 1987; Migowski *et al.* 2004; Ambraseys 2009). Most of the damages related to this earthquake are reported north of our site, with significant destructions in Jerusalem and in the citadel of Al-Karak (Fig. 1), which overlooks the southern Dead Sea basin from its eastern shoulder (Ambraseys 2009). This earthquake is recognized in most of the seismic sequences cored in the Dead Sea (Kagan *et al.* 2011), but is not formally identified south of the Dead Sea, at the site of Tilah (Fig. 1), although at that site obliteration of evidence by erosion cannot be totally excluded (Haynes *et al.* 2006). The city of Aqaba/Eilat, south of our site, was probably not significantly affected as no mention of damages related to this event has been found. This earthquake was weakly felt in Cairo, Egypt. Hence, the description of the destructions and our observations, all together suggest that this earthquake ruptured a section of the Wadi Araba fault located between our site and the southern tip of the Dead Sea (Fig. 7), although at this point it is impossible to ascertain with accuracy the northernmost limit of the 1458 rupture.

The penultimate event, E2, recorded at this site is constrained by several  $^{14}\text{C}$  samples located in units just below and above the event horizon. It had to occur between 1155 C.E. and 1269 C.E. According to historical chronicles the only possible earthquake is the earthquake that occurred on 1212 May 1. This earthquake produced extensive damages in the city of Aila (the ancient city corresponding to the modern Aqaba/Eilat) and to the Monastery of St Catherine located in Sinai. It was widely felt in Egypt, where many houses collapsed. Destructions were also reported north of the Wadi Araba, in Al-Karak and in Al-Shobak (Fig. 1), two cities located on the Jordan plateau, east of the Wadi Araba valley, between the Gulf of Aqaba and the Dead Sea (Ambraseys 2009). A brecciated layer is unambiguously associated to this event in the Dead Sea basin (Kagan *et al.* 2011). However, no ground rupture related to this event was identified at the trench site of Tilah (Fig. 1; Haynes *et al.* 2006), making unlikely the rupture of the entire Wadi Araba fault. The magnitude of this event, based on the reported damage and the area where the event was felt, is estimated to about  $M7.5$  (Migowski *et al.* 2004; Kagan *et al.* 2011). Based on observations at our site and the distribution of damages this earthquake was most probably located between our trench site and the Gulf of Aqaba (Fig. 7), with potential ruptures in the gulf as well.

The third event, E3, identified unambiguously, occurred between 1003 C.E. and 1138 C.E. This time window corresponds to the time of the 1068 C.E. seismic crisis that was widely documented in the area. Proper location of earthquakes associated to the crisis of 1068 C.E., however, has long been uncertain and disputed. A surface rupture has been tentatively associated to a 1068 C.E. earthquake at the Tilah site (Fig. 1) located about 15 km south of the Dead Sea (Haynes *et al.* 2006), but dating, based on a single sample, possibly reworked, remains weak. Reports of damages and felt effects cover a large area, from the northern Palestine to the city of Medina in Saudi Arabia: A large number of casualties

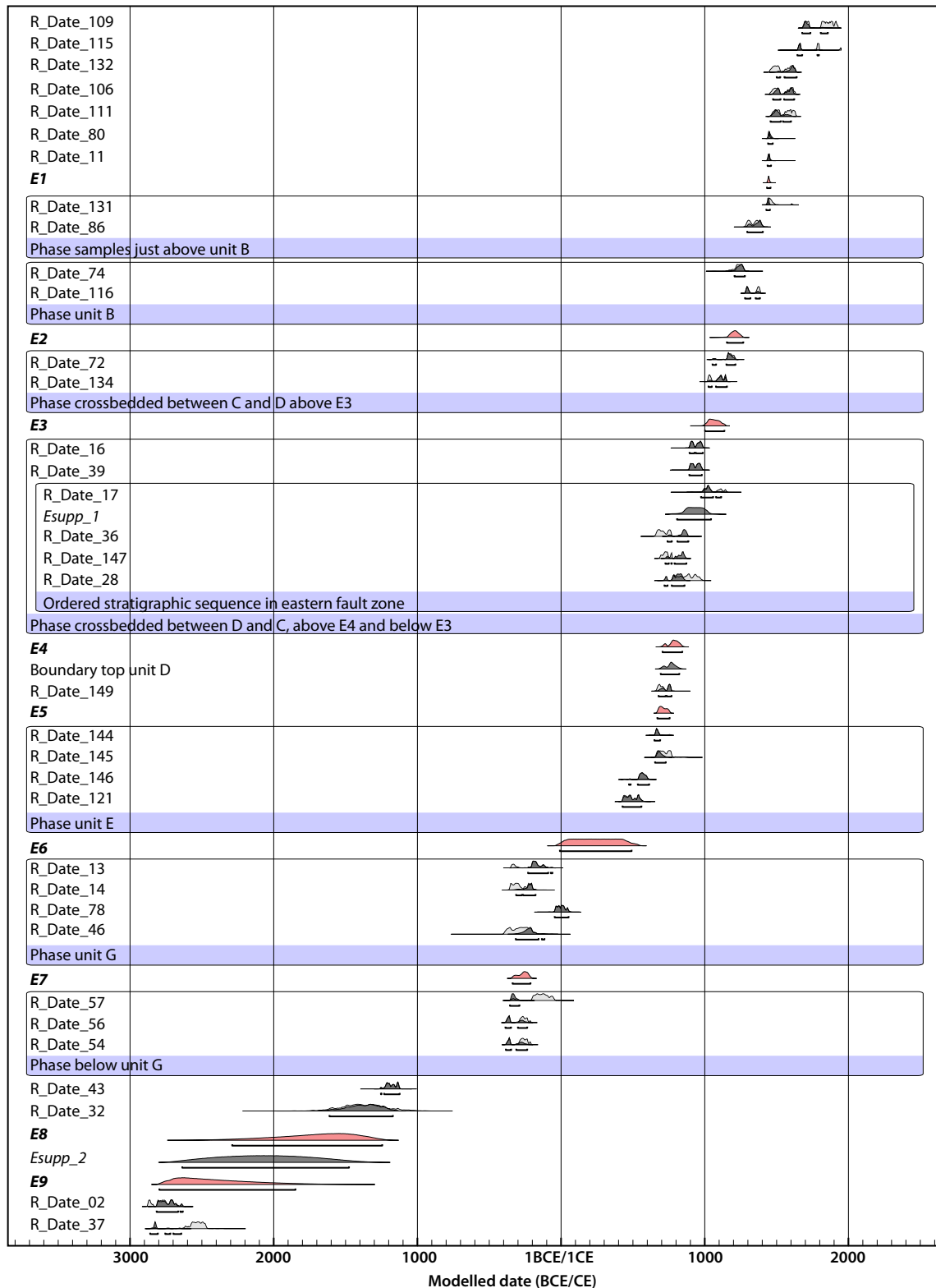


**Figure 6.** Age model computed for the trench stratigraphy using OxCal v4.2 (Bronk-Ramsey *et al.* 2010) and IntCal13 calibration curve (Reimer *et al.* 2013). Light grey indicates raw calibration and dark grey indicates modelled ages including stratigraphic information. Phases indicate subsets of samples where stratigraphic order is imposed.

(allegedly >10 000) have been reported in the city of Al-Ramla, north of Jerusalem, although some of the original chronicles have been deemed inaccurate, if not even false (Ambraseys 2009). Almost the entire population of Aila, on the seashore of the Gulf of

Aqaba, was killed, and damages to mosques were reported as far as Medina and Cairo (Ambraseys 2009). Hence, based on these historical reports a very large magnitude had been assigned to this earthquake and the epicentre could be located anywhere along the

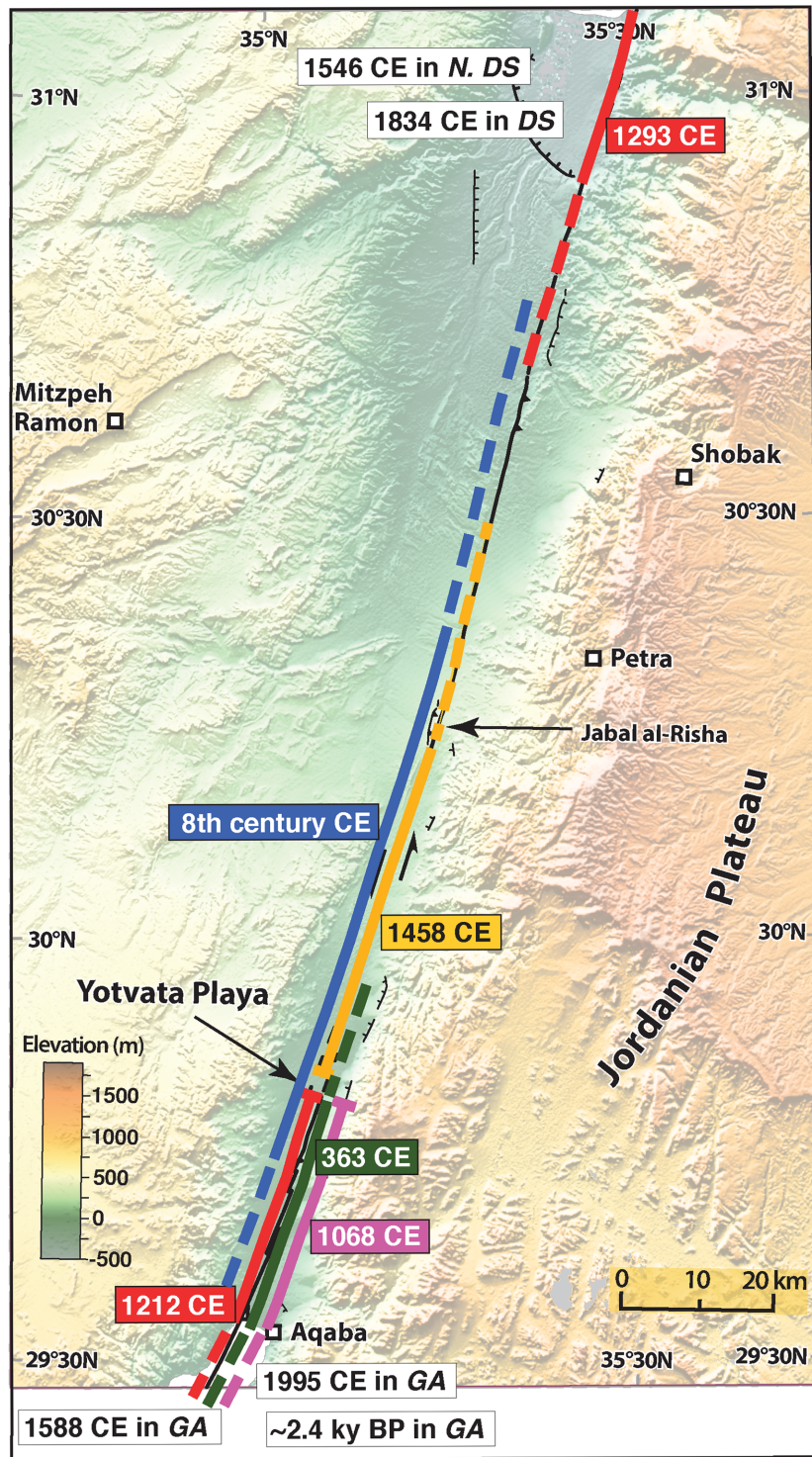


**Figure 7.** Lateral extent of historical earthquakes in the Wadi Araba based on events identified in the trench and on historical accounts. The Yotvata extensional jog appears to act like a stopping/initiation point for many ruptures, although larger earthquakes seem to be able to break through. Further studies are needed to detail seismic history of the Wadi Araba during the 8th century regional seismic crises and earlier in time. GA and N. DS stand for Gulf of Aqaba and Northern Dead Sea, respectively.

Dead Sea fault, between South Lebanon and the Gulf of Aqaba (Zilberman *et al.* 2005) and references herein). An epicentre was also suggested in the Hejaz mountains, northwest of Saudi Arabia, to account for the modification of water springs reported close to the city of Tabuk (Ambraseys *et al.* 1994). It was clearly established only recently (Guidoboni & Comastri 2005; Ambraseys 2009) that

reports from two distinct earthquakes, the 1068 March 18 event, most probably located south of the Dead Sea, and the 1068 May 29 event, located closer to northern Palestine, had been aggregated into a single giant earthquake in most of the historical accounts. (Kentor *et al.* 2001; Kagan *et al.* 2011). The total destruction of the city of Aila and of its local irrigation system (Zilberman *et al.* 2005;

Ambraseys 2009) added to the strength of shaking in Saudi Arabia and Egypt and to the surface rupture evidenced in our trench suggest that the 1068 March 18 earthquake was located in the southern Wadi Araba (Fig. 7). This earthquake would have ruptured, at least, the fault segments located between our site and the Gulf of Aqaba, that is about 30 km southward, leading to a magnitude  $M_w$  6.5 or higher (Wells & Coppersmith 1994), in good agreement with values proposed earlier, based on macroseismic reports and geomorphological observations (Abou Karaki 1987; Klinger *et al.* 2000b; Amit *et al.* 2002; Zilberman *et al.* 2005).

An earthquake, E<sub>supp1</sub>, possibly occurred between E3 and E4. As discussed earlier, evidence is scarce and visible unambiguously only in the eastern part of the trench. This event would have occurred between 806 C.E. and 1044 C.E. The age bracket excludes that it could be related to the 1068 C.E. earthquake series and no major earthquake is reported south of the Dead Sea basin during this period. Hence, these cracks could be related to shaking either associated to the earthquakes that affected the area of Tiberias in 850–854 C.E., or in 873 C.E. (Agnon 2014), or more probably to the earthquake of 1033 C.E. that severely affected the area north of the Dead Sea (Ambraseys 2009). This later earthquake, which was followed by numerous aftershocks, has caused severe destructions in several places in Palestine.

Events E4 and E5 are more difficult to tie to specific earthquakes recorded in historical chronicles. The two earthquakes had to happen very close in time as cracks associated with each event end within a very short distance in our trench. The existence of the distinct unit D, however, prevents any ambiguity about the fact that two distinct events are recorded here. Based on our age distribution (Fig. 6), the time bracket that includes the two earthquakes is 671 C.E.–845 C.E. Historical descriptions during this period, although numerous, are rather confused, due to the fact that different calendars were in use at the same time with no possible univocal date conversion between the different systems. In addition, early historians had a tendency to aggregate descriptions of different earthquakes into single giant earthquakes. Ambraseys (2009) demonstrated that at least three large earthquakes struck the region south of the Lebanese range between 746 C.E. and 757 C.E. Although damages are reported for many of the main cities of the region, it remains difficult to ascertain epicentral location for each of them based only on macroseismic data. Paleoseismological and numismatic findings suggest that at least one large event, in 749 C.E., took place south of Lake Tiberias, along the Jordan valley (Marco *et al.* 2003; Ferry *et al.* 2011; Kagan *et al.* 2011; Wechsler *et al.* 2014). Evidence at our trench site and evidence for damage in the ancient city of Aila (Thomas *et al.* 2007) during the same time window suggest one large earthquake in the southern part of the Dead Sea fault, E4, which caused major ground disruption. This event was preceded slightly earlier by another event, E5, of smaller magnitude, or alternatively quite distant, which triggered cracks with minor deformation at our site. Hence, a possible scenario would be a first major earthquake, E5, corresponding to 749 C.E., which ruptured fault segments north of the Dead Sea and was recorded only by few cracks at our trench site. In the following years, rupturing in a sequence, another large earthquake (E4) would rupture this time the southern section of the fault, with major ground deformation. At this stage, however, we cannot exclude an alternative scenario where the first event E5 does not correspond to the Jordan Valley 749 C.E. event, but to an event located further south, in the Gulf of Aqaba, similarly to  $M_w$  7.3 Nuweiba earthquake in 1995 (Klinger *et al.* 1999).

The time bracket for event E6 is large because we could not date the deposition of unit F, due to absence of preserved organic

material in this coarse sand unit, and we have ages only in unit E. Hence, the timing of E6 is constrained to be between 9 B.C.E. and 492 C.E. Although historical records are less numerous during this period, two historical earthquakes are reported in this time window, respectively in 115 C.E. and in 363 C.E. The first event, 115 C.E., is poorly documented and it has been suggested that war-related destructions and intermediate-magnitude earthquake effects were aggregated, leading to exaggerate the actual magnitude of earthquakes that occurred during that time (Ambraseys 2009). The event that occurred in 363 C.E. is better documented. It actually corresponds to two shocks separated by 6 hr during the night of 363 May 18. This seismic sequence is recorded in the varve sequence of the Dead Sea where a seismite could be unambiguously associated to this event (Kagan *et al.* 2011). According to historical descriptions, the second shock severely affected the southern part of the Dead Sea basin. A seiche was reported on the southeastern coast of the Dead Sea, as well as such destruction in southern Palestine localities and in the city of Petra (Ambraseys 2009). At the southern end of the Wadi Araba, in Aila, extensive destruction of Roman buildings is documented with the time of destruction well constrained to be post 360 C.E., according to dates of more than 100 coins found under collapsed walls (Thomas *et al.* 2007). Hence, the 363 C.E. seismic sequence seems to have affected significantly the southern part of the Dead Sea fault and most probably corresponds to our event E6, although further investigation would be needed to definitively rule out the possibility of 115 C.E.

The trench log (Fig. 5) allows for the identification of three, and possibly four more earthquakes, between 188 B.C.E. and 2798 B.C.E. The event E7 occurred during the period 338 B.C.E.–213 B.C.E. The sequence E8–E9 seems to have occurred in a pair during the period 2797 B.C.E.–1245 B.C.E. The supplementary event E<sub>supp2</sub> would also have occurred in this period. We cannot rule out that we might be missing earthquakes for the time period prior to E6, in part due to a large sedimentation rate in the lower western part of the trench, and in part because of erosion between units H and G, which has probably obliterated part of the record. However, because no obvious hiatus in the sedimentary column and in the age distribution is visible, it seems that our record could be complete, at least for the large events, for the last 5000 yr. Hence, the pairing of E8 and E9 might be possible and it would reflect the fact that earthquakes appear to happen during regional seismic crises such as the well-documented 8th century crisis or the 363 C.E. earthquake doublet.

Earthquakes E7–E9 are difficult to correlate with historically documented events. However, E7 and the sequence E8–E9 can be tentatively correlated to two successive down-faulting events along the northwestern tip of the Gulf of Aqaba, which have buried alive a coral-reef platform (Shaked *et al.* 2011). These two events have been dated using  $^{14}\text{C}$  and U-series on coral and yield ages of  $\sim 2.4$  ka BP and  $\sim 4.7$  ka BP, respectively, in agreement with the two seismic periods identified in the lower part of the trench (E7 and E8+E9). In addition, the date interval for event E7 is also compatible with a seismite layer dated about mid-2nd century B.C.E. that was consistently documented all around the Dead Sea basin, and was associated to a large magnitude event which would have affected the northern part of the Dead Sea fault (Kagan *et al.* 2011). The oldest sequence (E8+E9) could be related to some destruction reported in archeological sites north of the Dead Sea, along the Jordan valley, which were associated with seismic activity and dated between 1100 B.C.E. and 2600 B.C.E. (Ferry *et al.* 2011). The timing of this last sequence is also in good agreement with the occurrence of significant rock falls along the western shoulder

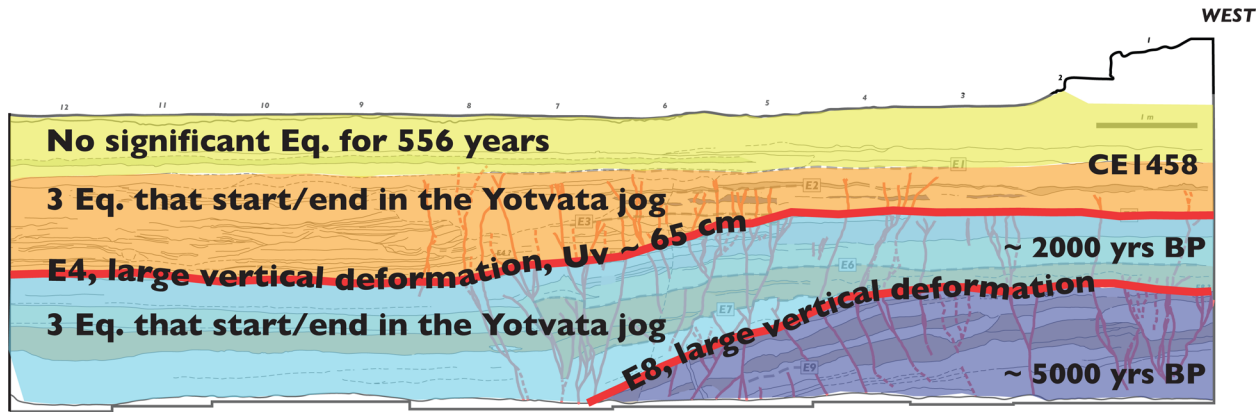


**Figure 8.** Some of the earthquakes identified at our trench site have produced major deformation, while others are only responsible for small vertical offsets and cracks. The later are assumed to stop/start in the Yotvata jog and the large one to break through it. The trench suggests that the fault alternates between periods with more numerous smaller events and periods with large less frequent events. Potentially 2 cycles could be observed in this trench. Uv strands for vertical deformation. Chronological indications are located at corresponding stratigraphic level.

of the Wadi Araba, dated to be  $4.3 \pm 1.0$  ka old, and which are associated to earthquake shaking (Matmon *et al.* 2005; Rinat *et al.* 2014). Hence, although these correlations are only qualitative at this point, they substantiate the assumption that the Dead Sea fault might be rupturing during seismic crises when several large earthquakes break different sections of the fault over a short period of a few centuries, separated by more quiet periods.

## DISCUSSION

In the Middle East, during the last 2000 yr, most of the significant earthquakes have been well recorded in historical accounts. However, the use of macroseismic data only has proved to be quite insufficient to locate specific earthquakes accurately, and additional paleoseismic data have often been decisive (Daëron *et al.* 2005, 2007). The situation of the southern section of the Dead Sea fault, in this respect, is even more difficult as the number of cities that could potentially report damages was always limited due to very arid climate. The new paleoseismological data exposed in our trench allow to identify several of the classic historical earthquakes and to constrain their area of rupture (Fig. 7). Historical earthquakes of 1458 C.E., 1212 C.E., 1068 C.E., one major earthquake during the 8th century seismic crisis of 746 C.E.–757 C.E., and the 363 C.E. event all ruptured the southern section of the Dead Sea fault, in the Wadi Araba. Interesting as well, some historical earthquakes have not been found at our trench site, meaning that they most probably ruptured other sections of the Dead Sea fault. The 1834 C.E. earthquake was widely felt in Palestine and caused some destruction in Jerusalem. Destructions are also reported East of the Dead Sea. Interestingly, it has been reported that large amount of asphalt was cast on the shore of the Dead Sea, suggesting that the earthquake could have been located in the Dead Sea or in direct vicinity (Ambraseys 2009; Agnon 2014). A ground rupture at the site of Tilah could also be correlated to this event although this correlation is far from being univocal (Haynes *et al.* 2006). Hence, for the 1834 event the location remains loosely constrained (Ambraseys 2009; Agnon 2014). The 1588 C.E. earthquake, which mostly affected the city of Aila and produced damage as far as Cairo in Egypt (Ambraseys 2009) was most likely limited to the Gulf of Aqaba (Agnon 2014), with no rupture propagating along the Wadi Araba section, similarly to the 1995 Nuweiba earthquake.

The 1546 C.E. earthquake is also not found in our trench. This event is classically described as an event that had affected the northern part of the Dead Sea basin. The southern extent of the rupture, however, is difficult to ascertain, as damage reports seem to have been grossly exaggerated (Ambraseys & Karcz 1992; Ambraseys 2009). Haynes *et al.* (2006) reported a ground rupture about 15 km south of the Dead Sea, at the Tilah site, that they associated to the earthquake of 1546 C.E. If this were to be confirmed, it would probably correspond to the southern end of the rupture. If conversely, as suggested by (Agnon 2014), the last rupture at Tilah is 1834 C.E., then the 1546 C.E. rupture would be limited to the Dead Sea basin only with no extension in the Wadi Araba. Finally, the 1293 C.E. earthquake is not found either in our trench. This is consistent with the fact that damages associated with this earthquake are mostly located north of the Wadi Araba, with the citadel of Al-Karak severely destroyed. More surprisingly, the 1293 C.E. rupture is not identified by Haynes *et al.* (2006), suggesting that this event would have been only limited to the Dead Sea basin, with no rupture along the Wadi Araba segments.

Among the several ruptures that we have identified at our trench site, the style and the size of the deformations differ significantly. The Dead Sea fault being a strike-slip fault, all the vertical deformations that are used here to identify events correspond only to secondary deformation, and a direct correlation of the amplitude of deformations with the events magnitude would be hazardous. Nevertheless, a first-order comparison between the deformation patterns (Fig. 8) might be indicative of some differences between the events that we have identified. The three most recent earthquakes identified in the trench are characterized by numerous cracks, but only small vertical offsets. In contrast, the 4th earthquake back in time, E4, in addition to the numerous cracks, is characterized by a large vertical deformation of about 65 cm. Although it is most probably due to local geometry of the fault, it is worth noting that it is the eastern side that went down, while at larger scale the basin associated to the extensional step over is located west of the fault. A similar pattern is visible for earlier events, although not so clear, with event E8 characterized by a large deformation and some block rotation, while the other events are mostly characterized by cracks. Although the smaller-deformation pattern could be due to variability of slip when earthquake rupture gets close to a jog (Klinger *et al.* 2006; Fletcher *et al.* 2014), it can alternatively be hypothesized that in most cases our site is close to the initiation or termination of an

earthquake rupture (Harris & Day 1999; Wesnousky 2006; Klinger 2010) and it would only record small deformation. In such cases, it means that these events actually ruptured only a limited section of the Wadi Araba fault during earthquakes of magnitude  $M_w$  6 to  $M_w$  7, quite in agreement with magnitude that could be inferred from historical descriptions (Abou Karaki 1987; Guidoboni *et al.* 1994; Guidoboni & Comastri 2005; Ambraseys 2009). Such earthquakes would be responsible for the typical 1 m to 1.5 m horizontal offset that can be observed ubiquitously along the Wadi Araba fault (Klinger *et al.* 2000b). In contrast, the larger deformation associated to E4 and E8 could indicate earthquakes that did not start/stop in the jog of Yotvata, but instead ruptured through. These events potentially broke a much longer section of the Wadi Araba fault, if not the entire 160-km-long Wadi Araba, during major earthquakes that could reach magnitude  $M_w$  7.5, with several metres of horizontal displacement (Wells & Coppersmith 1994). Such earthquakes could be part of earthquake series at the scale of the Dead Sea fault, producing regional earthquake turmoil, such as the one reported during the 8th century in the entire Middle East (Guidoboni *et al.* 1994; Ambraseys 2009).

In our record, the distribution of earthquakes through time, as well as the rupture size, seem to be variable. The early part of our record, between ~5000 yr BP and E6, ~1600 yr BP, shows only few earthquake bursts, at least about 500 yr apart. As we already acknowledged, we cannot exclude that we might miss some events in this time window, but we could not identify any obvious large hiatus in the sedimentary sequence, which should be easily detectable in the age distribution (Fig. 6). At about 1600 yr BP and the occurrence of earthquake E6, the seismic behaviour along the southern part of the Dead Sea fault seems to have switched to a different behaviour: The fault was producing earthquakes more often with reduced time interval between events, from 132 to 386 yr. Then, after the last significant earthquake in 1458 C.E., the fault behaviour seems to have changed to turn quiet again with no significant earthquake along the southern section of the Dead Sea fault for 556 yr. Using a slip rate of 5 mm yr<sup>-1</sup> (Le Béon *et al.* 2010), this corresponds to 2.8 m of accumulated slip, which would translate into an earthquake of magnitude  $M_w$  ~ 7 or higher (Wells & Coppersmith 1994; Le Béon *et al.* 2010). The only notable exception during the recent quiet period is the  $M_w$  7.3 earthquake that struck the Gulf of Aqaba in 1995 (Baer *et al.* 1999; Klinger *et al.* 1999; Hofstetter *et al.* 2003). It is yet too early to know if this most recent earthquake is starting a new series of events along the Dead Sea fault, or if it was just an anomaly during a long quiet period.

Alternation of intense seismic activity over a couple of centuries to a thousand years and period of seismic quiescence have been documented in several places along the Dead Sea fault, suggesting that it could correspond to its normal long-term seismic behaviour. From the Lebanese Range to the Gulf of Aqaba, four paleoseismological sites (Fig. 1) have time series that are long enough to compute a mean return time. The first site is located along the Yammounh fault section, in Lebanon (Daëron *et al.* 2005; Daëron *et al.* 2007). Up to 13 earthquakes have been identified at this site over a period of ~12 000 yr, with the last earthquake in 1202 C.E. The mean Return Interval (RI) is 940 yr with a standard deviation ( $\sigma$ ) of 424 yr. The Coefficient of Variation (CoV =  $\sigma$ /RI) is 0.45. The second site is located on the northern shore of Lake Tiberias. There, 8 events have been identified over a period of ~2000 yr, with the last earthquake in 1759 C.E. (Marco *et al.* 2005; Wechsler *et al.* 2014). RI is 207.4 yr and  $\sigma$  = 232.71 yr, yielding CoV of 1.13. The third site is located in the Jordan Valley. There, 12 events have been identified over a period of ~12 000 yr, with the last event possibly

in 1033 C.E. (Ferry *et al.* 2011). At that site RI is 1164 yr with  $\sigma$  = 807 yr and CoV = 0.7. Eventually, our site, located along the southern strand of the Dead Sea fault allows for identification of eight periods of seismic activity over ~5000 yr, with the last event in 1458 C.E. RI is 538 yr with  $\sigma$  = 420.9 yr and CoV = 0.78. If not identical, CoV at the different sites are consistent, with the exception of the site close to Lake Tiberias. There, conjunction of high detection level, shorter period considered compared to the other sites, and the peculiar location of the site at the junction between different segments (Wechsler *et al.* 2014) might be responsible for abnormally short RI and high CoV. This is probably enhanced by the fact that, at this stage, RI does not account for magnitude and considers all earthquakes similarly. The general picture, however, shows CoV  $\gg$  0 meaning that the Dead Sea fault departs significantly from a periodic seismic behaviour during the last millennia (Goes & Ward 1994; Zielke *et al.* 2015). In contrast, if one considers only the most recent series of earthquakes, E1–E6, at our site, which occurred over a period of about a thousand years, it yields a CoV = 0.34, indicative of a more periodic behaviour. Such difference shows how critical it is to get an earthquake time series long enough to evidence possible variability of the seismic behaviour with time.

Data-driven study (Marco *et al.* 1996; Agnon *et al.* 2006) and model-driven study (Kenner & Simons 2005; DiCaprio *et al.* 2008) both suggested that seismic activity along the Dead Sea fault might be clustered in time and space at the scale of tens of thousands of years. It seems from recent studies that it could also be the case at the timescale of a couple of thousands of years with entire sections of the Dead Sea fault switching from an active seismic mode to a more quiet mode (Ben-Zion *et al.* 1999).

## CONCLUSION

The number of strike-slip faults where the earthquake record is long enough to be able to study fault seismic behaviour remains very small. Although attempts have been numerous, sites that preserved a long record of past earthquakes and enough material suitable for dating are difficult to find. Here, we present a site located at the southern end of the on-land part of the Dead Sea fault where we could identify up to nine events grouped in eight bursts of activity, over a period of about 5000 yr. Several of these earthquakes can be tied to historical earthquakes in chronicles, but for which location was remaining uncertain until now. The series of earthquakes recorded at our site, along with earthquakes recorded at three other sites further north along the Dead Sea fault, show some variability in the time distribution of earthquakes, with period of intense activity over few centuries and period of seismic quiescence. In addition, the fact that we observe several pairs of earthquakes, which occurred only few years to few decades apart, suggests that during periods of seismic activity, rupture of one section of the Dead Sea fault might trigger rupture on other nearby fault sections, leading to the total rupture of the Dead Sea fault in a relatively short time of few centuries. Such pattern of temporal clustering is not unique to the Dead Sea fault and it has been unambiguously evidenced along other large strike-slip fault such as the North Anatolian Fault, in Turkey (Barka 1996; Stein *et al.* 1997), and the San Jacinto fault, in United States (Rockwell *et al.* 2014). In contrast, however, other records along the Alpine fault, in New Zealand (Berryman *et al.* 2012) and the San Andreas fault, in United States (Scharer *et al.* 2010), show that on these faults the seismicity might be quasi-periodic in time. Hence, time clustering does not seem to be an intrinsic behaviour of

strike-slip faults. Because one could not do any obvious correlation between a specific earthquake behaviour and a simple property of the system, such as fault geometry or isolation of the fault system relatively to other active faults, we suggest instead that it is more likely that the key to temporal clustering might depend on some relation between slip-rate and the existence of a time-dependent rheology (a rheology that would keep memory of earthquake history) in the lower crust and the upper mantle, as suggested in several model-driven approaches (Ben-Zion *et al.* 1999; Lyakhovskiy *et al.* 2001; Kenner & Simons 2005; DiCaprio *et al.* 2008).

## ACKNOWLEDGEMENTS

The authors would like to thank Myrtille Kupermink who was involved in the fieldwork and some preliminary analyses. We thank C. Gruetznier, A. Agnon and U. Weckmann for their thoughtful reviews and comments that improved this manuscript. This project was partly funded by the Libris project (ANR-09-RISK-006) and by Jordan Areva Ressources. MLB thanks post-doctorate advisor John Suppe for financial support. IPGP contribution 3619.

## REFERENCES

- Abou Karaki, N., 1987. Synthèse et carte sismotectonique des pays de la bordure orientale de la Méditerranée: sismicité du système de failles du Jourdain—Mer Morte, *PhD*, Université Louis Pasteur de Strasbourg.
- Agnon, A., 2014. 8 Pre-instrumental earthquakes along the Dead Sea transform, in *Dead Sea Transform Fault System: Reviews*, pp. 207–261, eds Garfunkel, Z., Ben Avraham, Z. & Kagan, E., Springer.
- Agnon, A., Migowski, C. & Marco, S., 2006. Intraclast breccias in laminated sequences reviewed: recorders of paleo-earthquakes, *Geol. Soc. Am. Spec. Papers*, **401**, 195–214.
- Alchalbi, A. *et al.*, 2010. Crustal deformation in the northwestern Arabia from GPS measurements in Syria: slow slip rate along the northern Dead Sea Fault, *Geoph. J. Int.*, **180**, 125–135.
- Ambraseys, N., 2009. *Earthquakes in the Mediterranean and Middle East: A Multidisciplinary Study of Seismicity up to 1900*, Cambridge Univ. Press.
- Ambraseys, N. & Karcz, I., 1992. The earthquake of 1546 in the Holy Land, *Terra Nova*, **4**, 254–263.
- Ambraseys, N., Melville, C. & Adams, D., 1994. *The Seismicity of Egypt, Arabia and the Red Sea*, Cambridge Univ. Press.
- Amit, R., Zilberman, E., Enzel, Y. & Porat, N., 2002. Paleoseismic evidence for time dependency of seismic response on a fault system in the southern Arava Valley, Dead Sea rift, Israel, *Geol. Soc. Am. Bull.*, **114**, 192–206.
- Baer, G., Sandwell, D., Williams, S., Bock, Y. & Shamir, G., 1999. Coseismic deformation associated with the November 1995,  $M_w = 7.1$  Nuweiba earthquake, Gulf of Elat (Aqaba), detected by synthetic aperture radar interferometry, *J. geophys. Res.*, **104**, 25 221–225 232.
- Barka, A., 1996. Slip distribution along the North Anatolian fault associated with the large earthquakes of the period 1939–1967, *Bull. seism. Soc. Am.*, **86**, 1238–1254.
- Ben Avraham, Z., 1992. Development of asymmetric basins along continental transform faults, *Tectonophysics*, **215**, 209–220.
- Ben-Zion, Y., Dahmen, K., Lyakhovskiy, V., Ertas, D. & Agnon, A., 1999. Self-driven mode switching of earthquake activity on a fault system, *Earth planet. Sci. Lett.*, **172/1–2**, 11–21.
- Berryman, K.R., Cochran, U.A., Clark, K.J., Biasi, G.P., Langridge, R. & Villamor, P., 2012. Major earthquakes occur regularly on an isolated plate boundary fault, *Science*, **336**, 1690–1693.
- Bronk-Ramsey, C., 2009. Bayesian analysis of radiocarbon dates, *Radiocarbon*, **51**, 337–360.
- Bronk-Ramsey, C., Dee, M., Lee, S., Nakagawa, T. & Staff, R., 2010. Developments in the calibration and modelling of radiocarbon dates, *Radiocarbon*, **52**, 953–961.
- Daëron, M., Benedetti, L., Tapponnier, P., Surssock, A. & Finkel, R., 2004. Constraints on the post ~25-ka slip rate of the Yammounh fault (Lebanon) using in-situ cosmogenic  $Cl^{36}$  dating of offset limestone clast fans, *Earth planet. Sci. Lett.*, **227**, 105–119.
- Daëron, M., Klinger, Y., Tapponnier, P., Elias, A., Jacques, E. & Surssock, A., 2005. Sources of the large AD1202 and 1759 Near East earthquakes, *Geology*, **33**, 529–532.
- Daëron, M., Klinger, Y., Tapponnier, P., Elias, A., Jacques, E. & Surssock, A., 2007. 12 000-year-long record of up to 14 paleo-earthquakes on the Yammouneh fault (Levant fault system), *Bull. seism. Soc. Am.*, **97**, 749–771.
- DiCaprio, C.J., Simons, M., Kenner, S.J. & Williams, C.A., 2008. Post-seismic reloading and temporal clustering on a single fault, *Geophys. J. Int.*, **172**, 581–592.
- Elias, A. *et al.*, 2007. Active thrusting offshore Mount Lebanon: source of the tsunamigenic, 551 AD Beirut-Tripoli earthquake, *Geology*, **35**, 755–758.
- Ferry, M., Meghraoui, M., Abou Karaki, N., Al-Taj, M. & Khalil, L., 2011. Episodic behavior of the Jordan valley section of the Dead Sea fault inferred from a 13-ka-long integrated catalog of large earthquakes, *Bull. seism. Soc. Am.*, **101**, 39–67.
- Fletcher, J.M. *et al.*, 2014. Assembly of a large earthquake from a complex fault system: surface rupture kinematics of the 4 April 2010 El Mayor–Cucapah (Mexico) Mw 7.2 earthquake, *Geosphere*, **10**, 797–827.
- Freund, R., Zak, I. & Garfunkel, Z., 1968. Age and rate of the sinistral movement along the Dead Sea rift, *Nature*, **220**, 527–538.
- Garfunkel, Z., 1981. Internal structure of the Dead Sea leaky transform (Rift) in relation to plate kinematics, *Tectonophysics*, **80**, 81–108.
- Garfunkel, Z., Zak, I. & Freund, R., 1981. Active faulting in the Dead Sea rift, *Tectonophysics*, **80**, 1–26.
- Goes, S. & Ward, S.N., 1994. Synthetic seismicity for the San Andreas fault, *Ann. Geophys.*, **37**, 1495–1513.
- Gomez, F. *et al.*, 2007. Global Positioning System measurements of strain accumulation and slip transfer through the restraining bend along the Dead Sea fault system in Lebanon, *Geophys. J. Int.*, **168**, 1021–1028.
- Guidoboni, E. & Comastri, A., 2005. *Catalogue of Earthquakes and Tsunamis in the Mediterranean Area from the 11th to 15th Century*, Istituto Nazionale di Geofisica & Vulcanologia.
- Guidoboni, E., Comastri, A. & Traina, G., 1994. *Catalogue of Ancient Earthquakes in the Mediterranean Area up to the 10th Century*, Istituto Nazionale di Geofisica.
- Haberland, C. *et al.*, 2007. Shallow architecture of the Wadi Araba fault (Dead Sea Transform) from high-resolution seismic investigations, *Tectonophysics*, **432**, 37–50.
- Harris, R. & Day, S., 1999. Dynamic 3D simulations of earthquakes on en echelon faults, *Geophys. Res. Lett.*, **26**, 2089–2092.
- Haynes, J.M., Niemi, T.M. & Atallah, M., 2006. Evidence for ground-rupturing earthquakes on the Northern Wadi Araba fault at the archaeological site of Qasr Tilah, Dead Sea transform fault system, Jordan, *J. Seismol.*, **10**, 415–430.
- Heimann, A. & Ron, H., 1993. Geometric changes of plate boundaries along part of the northern Dead Sea transform: geochronologic and paleomagnetic evidence, *Tectonics*, **12**, 477–491.
- Hofstetter, A., Thio, H.K. & Shamir, G., 2003. Source mechanism of the 22/11/1995 Gulf of Aqaba earthquake and its aftershock sequence, *J. Seismol.*, **7**, 99–114.
- Kagan, E., Stein, M., Agnon, A. & Neumann, F., 2011. Intra-basin paleo-earthquake and quiescence correlation of the late Holocene Dead Sea, *J. geophys. Res.*, **116**, doi:10.1029/2010JB007452.
- Kenner, S.J. & Simons, M., 2005. Temporal clustering of major earthquakes along individual faults due to post-seismic reloading, *Geophys. J. Int.*, **160**, 179–194.
- Ken-Tor, R., Agnon, A., Enzel, Y., Stein, M., Marco, S. & Negendank, J.F.W., 2001. High-resolution geological record of historic earthquakes in the Dead Sea basin, *J. geophys. Res.: Solid Earth*, **106**, 2221–2234.
- Kesten, D., Weber, M., Haberland, C., Janssen, C., Agnon, A., Bartov, Y., Rabba, I. & Group, D., 2008. Combining satellite and seismic images

- to analyse the shallow structure of the Dead Sea Transform near the DESERT transect, *Int. J. Earth Sci.*, **97**, 153–169.
- Klinger, Y., 2010. Relation between continental strike-slip earthquake segmentation and thickness of the crust, *J. geophys. Res.*, **115**, doi:10.1029/2009JB006550.
- Klinger, Y., Rivera, L., Haessler, H. & Maurin, J., 1999. Active faulting in the Gulf of Aqaba: new knowledge from the  $M_w$  7.3 earthquake of 22 November 1995, *Bull. seism. Soc. Am.*, **89**, 1025–1036.
- Klinger, Y., Avouac, J.P., Abou Karaki, N., Dorbath, L., Bourles, D. & Reyss, J.L., 2000a. Slip rate on the Dead Sea transform fault in northern Arava Valley (Jordan), *Geophys. J. Int.*, **142**, 755–768.
- Klinger, Y., Avouac, J.P., Dorbath, L., Abou Karaki, N. & Tisnerat, N., 2000b. Seismic behaviour of the Dead Sea Fault along Arava Valley, Jordan, *Geophys. J. Int.*, **142**, 769–782.
- Klinger, Y., Michel, R. & King, G.C.P., 2006. Evidence for an earthquake barrier model from Mw similar to 7.8 Kokoxili (Tibet) earthquake slip-distribution, *Earth planet. Sci. Lett.*, **242**, 354–364.
- Le Béon, M. *et al.*, 2008. Slip rate and locking depth from GPS profiles across the southern Dead Sea Transform, *J. geophys. Res.*, **113**, B11403, doi:10.1029/2007JB005280.
- Le Béon, M. *et al.*, 2010. Early Holocene and late Pleistocene slip rate of the southern Dead Sea fault determined by  $^{10}\text{Be}$  cosmogenic dating of offset alluvial deposits, *J. geophys. Res.*, **115**, doi:10.1029/2009JB007198.
- Le Béon, M., Klinger, Y., Meriaux, A.S., Al-Qaryouti, M., Finkel, R.C., Mayyas, O. & Tapponnier, P., 2012. Quaternary morphotectonic mapping of the Wadi Arava and implications for the tectonic activity of the southern Dead Sea fault, *Tectonics*, **31**, doi:10.1029/2012TC003112.
- Lienkaemper, J.J. & Bronk-Ramsey, C., 2009. OxCal: Versatil tool for developing paleoearthquake chronologies—a primer, *Seism. Res. Lett.*, **80**, 431–434.
- Liu-Zeng, J., Shao, Y., Klinger, Y., Xie, K., Yuan, D. & Lei, Z., 2013. Paleo-earthquakes of diverse magnitude recorded at the Salt Lake site, the Haiyuan Fault, China, in *Proceedings of the AGU Fall Meeting*, San Francisco.
- Lyakhovskiy, V., Ben-Zion, Y. & Agnon, A., 2001. Earthquake cycle, fault zones, and seismicity patterns in a theologically layered lithosphere, *J. geophys. Res.*, **106**, 4103–4120.
- Makovsky, A., Wunch, A., Ariely, R., Shaked, Y., Rivlin, A., Shemesh, A., Ben Avraham, Z. & Agnon, A., 2008. Quaternary transform kinematics constrained by sequence stratigraphy and submerged coastline features: the Gulf of Aqaba, *Earth planet. Sci. Lett.*, **271**, 109–122.
- Marco, S. & Klinger, Y., 2014. 7 Review of on-fault palaeoseismic studies along the Dead Sea fault, in *Dead Sea Transform Fault System: Reviews*, pp. 183–205, eds Garfunkel, Z., Ben Avraham, Z. & Kagan, E., Springer.
- Marco, S., Stein, M., Agnon, A. & Ron, H., 1996. Long-term earthquake clustering: a 50 000-year paleoseismic record in the Dead Sea Graben, *J. geophys. Res.*, **101**(B3), 6179–6191.
- Marco, S., Hartal, M., Hazan, N., Lev, L. & Stein, M., 2003. Archaeology, history, and geology of the A.D. 749 earthquake, Dead Sea transform, *Geology*, **31**, 665–668.
- Marco, S., Rockwell, T., Heimann, A. & Frieslander, U., 2005. Late Holocene slip of the Dead Sea transform revealed in 3D paleoseismic trenches on the Jordan Gorge fault, *Earth planet. Sci. Lett.*, **234**, 189–205.
- Matmon, A., Shaked, Y., Agnon, A., Porat, N., Enzel, Y., Finkel, R., Lifton, N. & Boarretto, E., 2005. Lessons to exposure age dating from constraining the time of earthquake induced rockfalls along the margins of the Dead Sea fault system, southern Israel, *Earth planet. Sci. Lett.*, **240**, 803–817.
- McCalpin, J., 1996. Paleoseismology, in *International Geophysics Series*, pp. 588, eds Dmowska, D. & Holton, J., Academic Press.
- Meghraoui, M. *et al.*, 2003. Evidence for 830 years of seismic quiescence from palaeoseismology, archaeoseismology and historical seismicity along the Dead Sea fault in Syria, *Earth planet. Sci. Lett.*, **210**, 35–52.
- Migowski, C., Agnon, A., Brookman, R., Negendank, J.F.W. & Stein, M., 2004. Recurrence pattern of Holocene earthquakes along the Dead Sea transform revealed by varve-counting and radiocarbon dating of lacustrine sediments, *Earth planet. Sci. Lett.*, **222**, 301–314.
- Niemi, T.M., Zhang, H.W., Atallah, M. & Harrison, J.B.J., 2001. Late Pleistocene and Holocene slip rate of the Northern Wadi Arava fault, Dead Sea Transform, Jordan, *J. Seismol.*, **5**, 449–474.
- Quennell, A., 1959. Tectonics of the Dead Sea rift, in *Proceedings of the Cong. Geological International XX Session*, Mexico, pp. 385–405.
- Reimer, P.J. *et al.*, 2013. IntCal13 and Marine13 radiocarbon age calibration curves 0–50 000 years cal BP, *Radiocarbon*, **55**, 1869–1887.
- Rinat, Y. *et al.*, 2014. Holocene rockfalls in the southern Negev Desert, Israel and their relation to Dead Sea fault earthquakes, *Quarter. Res.*, **81**, 260–273.
- Rockwell, T.K., Dawson, T.E., Ben-Horin, J.Y. & Seitz, G., 2014. A 21-event, 4000-year history of surface ruptures in the Anza Seismic Gap, San Jacinto Fault, and implications for long-term earthquake production on a major plate boundary fault, *Pure appl. Geophys.*, 1–23.
- Scharer, K.M., Biasi, G.P., Weldon, R.J. II. & Fumal, T.E., 2010. Quasi-periodic recurrence of large earthquakes on the San Andreas fault, *Geology*, **38**, 555–558.
- Shaked, Y., Lazar, B., Marco, S., Stein, M. & Agnon, A., 2011. Late Holocene events that shaped the shoreline at the northern Gulf of Aqaba recorded by a buried fossil reef, *Isr. J. Earth. Sci.*, **58**, 355–368.
- Stein, R., Barka, A. & Dieterich, J., 1997. Progressive failure on the North Anatolian fault since 1939 by earthquake stress triggering, *Geophys. J. Int.*, **128**, 594–604.
- Stuiver, M. & Polach, H.A., 1977. Discussion reporting of  $^{14}\text{C}$  data, *Radiocarbon*, **19**, 355–363.
- Thomas, R., Parker, S.T. & Niemi, T.M., 2007. Structural damage from earthquakes in the second-ninth centuries at the archaeological site of Aila in Aqaba, Jordan, *Basor*, **346**, 59–77.
- Wechsler, N., Rockwell, T., Klinger, Y., Stepancikova, P., Kanari, M., Marco, S. & Agnon, A., 2014. A paleoseismic record of earthquakes for the Dead Sea transform fault between the first and seventh centuries C.E.: nonperiodic behavior of a plate boundary fault, *Bull. seism. Soc. Am.*, **104**, doi:10.1785/0120130304.
- Wells, D.L. & Coppersmith, K.J., 1994. New empirical relationships among magnitude, rupture length, rupture width, rupture area, and surface displacement, *Bull. seism. Soc. Am.*, **84**, 974–1002.
- Wesnousky, S., 2006. Predicting the endpoints of earthquake ruptures, *Nature*, **444**, 358–360.
- Zielke, O., Klinger, Y. & Arrowsmith, J.R., 2015. Earthquake (recurrence) characteristics revealed by high-resolution topographic data, *Tectonophysics*, **638**, 43–62.
- Zilberman, E., Amit, R., Porat, Y., Enzel, Y. & Avner, U., 2005. Surface ruptures induced by the devastating 1068AD earthquake in the southern Arava valley, Dead Sea Rift, Israel, *Tectonophysics*, **408**, 79–99.

## SUPPORTING INFORMATION

Additional Supporting Information may be found in the online version of this paper:

**Figure S1.** Photomosaic of the trench wall. Each square is 1 m per side (<http://gji.oxfordjournals.org/lookup/suppl/doi:10.1093/gji/ggv134/-DC1>).

Please note: Oxford University Press is not responsible for the content or functionality of any supporting materials supplied by the authors. Any queries (other than missing material) should be directed to the corresponding author for the paper.